Phase Transition and Electric Conductivity of $ASnCl_3$ (A = Cs and CH_3NH_3)

Koji Yamada,* Yasuhisa Kuranaga, Keita Ueda, Shusaku Goto, Tsutomu Okuda, and Yoshihiro Furukawa†

Department of Chemistry, Faculty of Science, Hiroshima University, Kagamiyama 1-3, Higashi-Hiroshima 739

†Faculty of School Education, Hiroshima University, Kagamiyama 1-1, Higashi-Hiroshima 739

(Received May 16, 1997)

A first-order phase transition of $CsSnCl_3$ to a cubic perovskite phase was observed at $T_{tr} = 379$ K. The electric conductivity increased from 10^{-6} S cm^{-1} to 10^{-3} S cm^{-1} at the phase transition. The temperature dependence of the electric conductivity and the X-ray diffraction data for $CsSnCl_3$ suggested a reconstructive nature of the phase transition. On the other hand, $CH_3NH_3SnCl_3$ showed successive phase transitions at 283, 307, 331, and 463 K with increasing temperature. The highest temperature phase belongs to a cubic perovskite structure, and pyramidal $SnCl_3^-$ anion exists below 465 K having distorted perovskite structures. The ^{119}Sn NMR spectra for $CH_3NH_3SnCl_3$ supported the coordination change around the Sn atom, and also suggested the onset of chloride-ion diffusion just below the phase-transition temperature to the cubic phase. The activation energy for chloride-ion diffusion was found to be 54 kJ mol^{-1} by analyzing the temperature dependence of ^{119}Sn NMR T_1. The electric conductivity of Cs and CH_3NH_3 salts, however, is governed by the semiconducting property of these compounds.

In previous papers we reported on the successive phase transitions and drastic increase in the electric conductivity for $CH_3NH_3GeCl_3$ at the phase transition to the cubic perovskite phase.[1,2] The high conductivity was attributed to the transport of the chloride ions on the basis of the ^{35}Cl NMR experiment. The Rietveld refinements of the X-ray powder diffraction data also supported the chloride ion conductor because a disorder at the Cl sites was confirmed. This type of disorder reflects the characteristic nature of the hypervalent bond formed in Sn(II), Ge(II), and Sb(III) compounds. That is, the cubic perovskite phase appears as the results of bond switching, Cl–Ge···Cl ⟷ Cl···Ge–Cl. On the other hand, a perovskite halide, such as $CsSnI_3$, $CH_3NH_3SnI_3$ or $CsSnBr_3$, showed a black color with semi-metallic conductivity.[3—5] In these semi-metallic compounds, –X–Sn–X– chains are formed throughout the crystal three-dimensionally. It is particularly interesting that two different types of conductivities, electronic and ionic-conductivities, appear in these perovskite halides. As long as a perovskite structure is maintained, a smaller cation is desired for a high electronic conductor, because the strong overlap of the atomic orbitals on adjacent atoms leads to an electronic structure having a broad band. However, for the design of a high ionic conductor, such as seen in $CH_3NH_3GeCl_3$, a suitable size of cation is required to stabilize the disordered state in the perovskite lattice.[1,2,6]

In this work we synthesized several trichlorostannate(II) salts and examined the electric properties of these salts by comparing previous studies concerning $ASnX_3$[3—5] and $AGeX_3$ (X = Cl and Br).[1,2,6]

Experimental

$RSnCl_3$ (R = alkylammonium) was synthesized by a solid-state reaction between alkylammonium chloride and $SnCl_2$ purified by a bridgman or zonemelting technique before use. The crystals of $CsSnCl_3$ were grown from a melt containing stoichiometric amounts of CsCl and $SnCl_2$. DTA was observed by a homemade apparatus. The heating rate was programmed to be 4 K min^{-1} by a temperature controller. Since the cooling curve was observed under spontaneous cooling in a dewer vessel, there was no qualitative relation among the perk area. The conductivity was determined by a complex impedance method (ANDO AG-4311B, frequency range from 100 to 100 kHz) for a pressed powder pellet coated with carbon electrodes on both sides. Powder X-ray diffraction was observed by a Rigaku Rad-B system with a homemade high-temperature cell using Cu $K\alpha$ radiation with a graphite monochrometor. The diffraction patterns were analyzed by a Rietveld method using a program developed by Izumi.[7] ^{2}H, ^{119}Sn NMR and NQR experiments were performed using Matec pulsed spectrometers under 6.37 T and without a field, respectively. ^{1}H NMR was observed at 1.41 T by a CW spectrometer in the temperature range from 290 to 473 K at the Instrument Center for Chemical Analysis, Hiroshima University.

Results and Discussion

Phase Transitions and Conductivities of Trichlorostannate(II) Salts. Figure 1 shows the DTA curves for $CsSnCl_3$ and $CH_3NH_3SnCl_3$. A 1st-order phase transition was detected for $CsSnCl_3$ at 379 K together with a color change from colorless to pale yellow. In the cooling process, this high-temperature phase (Phase I) showed two exother-

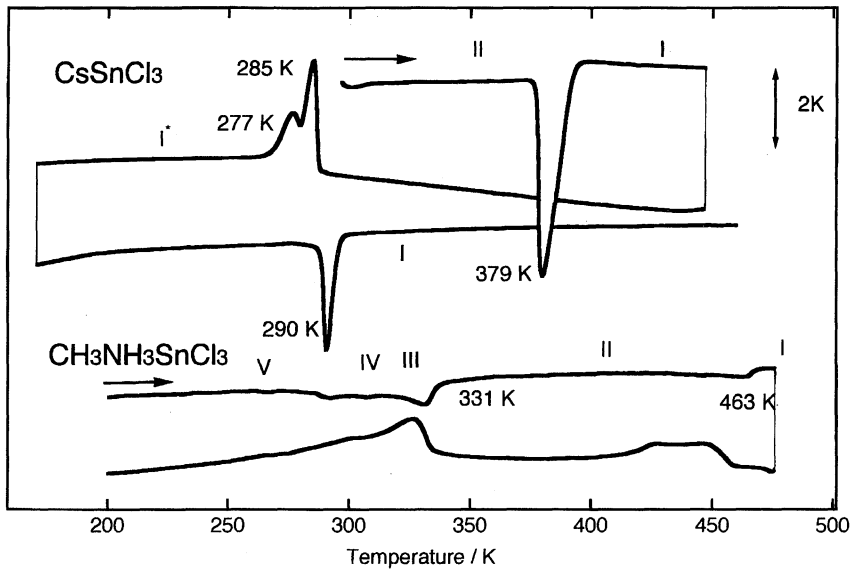

Fig. 1. DTA curves for $CsSnCl_3$ and $CH_3NH_3SnCl_3$. The transition temperatures were determined at the peak positions using the heating curves. Heating rate 4 K min^{-1}.

mic peaks at 285 and 277 K without any change in the color. With heating again, this pale-yellow phase changed to Phase I at 290 K, which was ca. 90 K lower than that of the Phase II to Phase I transition. These findings suggested that the low-temperature phase appearing on the DTA curve can be assigned to a metastable phase. The metastable phase was abbreviated as Phase I*. A distinct ^{35}Cl NQR spectrum for Phase I* from that of the phase II also supported the metastable phase. On the other hand, $CH_3NH_3SnCl_3$ showed complex phase changes between 250 and 480 K. The endothermic peak at 331 K has a long tail at the lower temperature side, suggesting an order-disorder character. Two small endothermic peaks at 283 and 307 K were superposed on the tail. These five phases were tentatively designated as Phase I, II, etc. from the high-temperature side.

Figure 2 reproduced the temperature dependencies of the conductivities for $CsSnCl_3$ and $CH_3NH_3SnCl_3$. The conductivity for $CH_3NH_3SnCl_3$ increased continuously with increasing temperature, and there was no discontinuity at T_{tr}. On the other hand, the complex impedance plot for Cs salt changed drastically around T_{tr}, as shown in Fig. 3. The resultant bulk conductivity, which was determined by assuming an equivalent circuit shown in Fig. 3, increased from 10^{-6} S cm^{-1} to 10^{-3} S cm^{-1} at T_{tr}. A preliminary conductivity measurement using a d.c. current at their cubic phases showed no polarization effect like that usually observed for ionic conductors. This suggests that the semiconducting property governs the electric conductivity as well as in perovskite $CH_3NH_3SnBr_3$.[8] Although the conductivity of $CsSnCl_3$ remained high in the cooling process, because of the quenching of Phase I, it gradually decreased at around room temperature. After ca. 24 h the conductivity decreased to that of Phase II, and a similar hysteresis loop was reproducible. This suggested that the phase transition from Phase I to II took place slowly at R.T.

Phase transitions were also observed for other alkylammonium salts by means of DTA. The transition temperatures are 380 K for $(CH_3)_2NH_2SnCl_3$, 277, 399, and 490 K for $(CH_3)_3NHSnCl_3$ and 236 K for $(CH_3)_4NSnCl_3$. No cubic perovskite phase was found for these samples below 490 K.

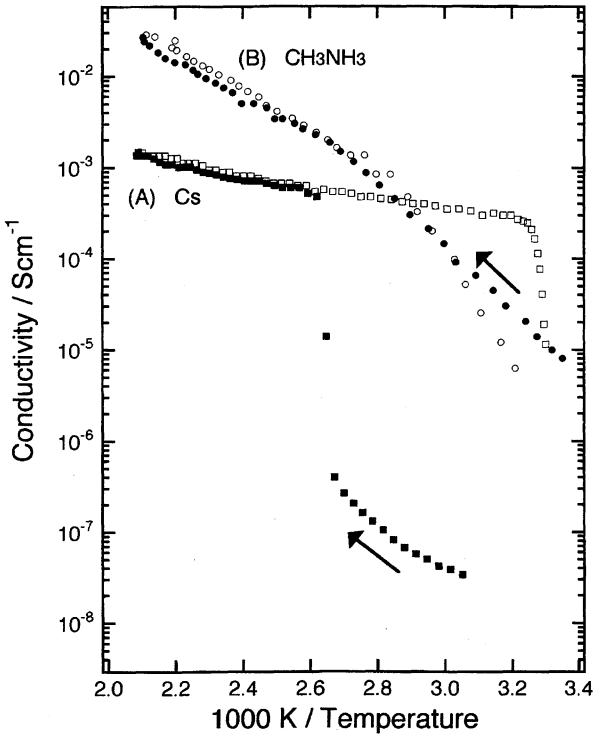

Fig. 2. Temperature dependence of conductivity determined by a complex impedance method. (A) $CsSnCl_3$ and (B) $CH_3NH_3SnCl_3$.

Crystal Structures of $CsSnCl_3$ and $CH_3NH_3SnCl_3$. The crystal of $CsSnCl_3$ belongs to a monoclinic system (space group $P2_1/n$) with $a = 16.10$, $b = 7.425$, $c = 5.748$ Å, and $\beta = 93.20°$.[9] It consists of a Cs^+ ion and an iso-

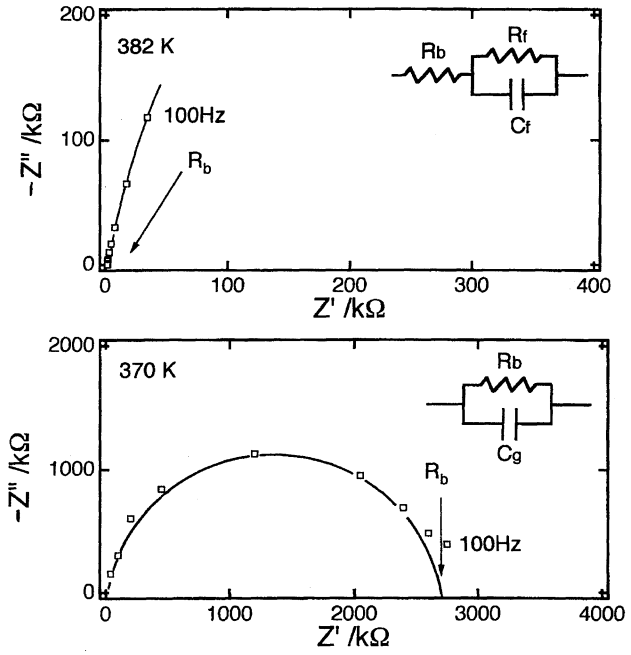

Fig. 3. Complex impedance plots for $CsSnCl_3$ just below and above T_{tr}. The equivalent circuits assumed are shown, where R_b is a bulk resistance, R_f is a resistance at the electrode surface, C_f is a capacitance between sample and electrode and C_g is a geometrical capacitance of the sample pellet.

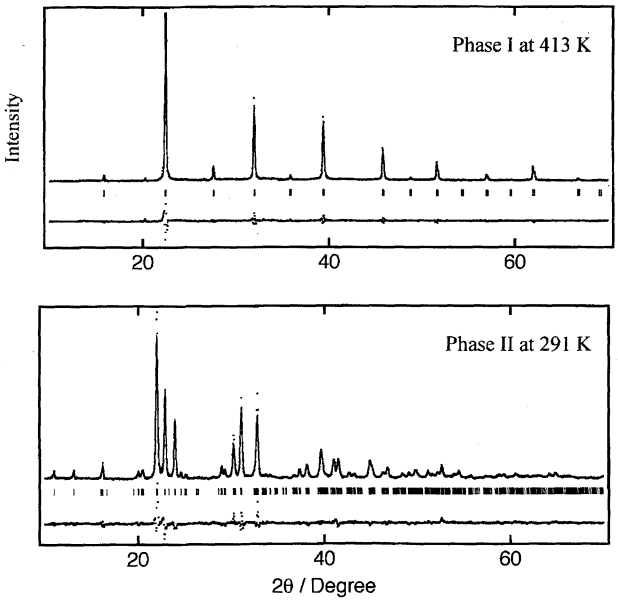

Fig. 4. Rietveld refinement plots for $CsSnCl_3$ at Phase I and II.

lated $SnCl_3^-$ anion, which forms a trigonal pyramid (Sn–Cl: 2.50—2.55 Å) having three long interanionic interactions (Sn···Cl: 3.21—3.77 Å). As the result of these interactions, the Sn forms distorted octahedral coordination. The XRD pattern at 291 K agreed well with the calculated one, as shown in Fig. 4. At T_{tr} the XRD pattern changed drastically together with a color change. The XRD pattern above T_{tr} supported the phase transition to a cubic perovskite phase, as already reported by Sharma.[10] From a comparison between the structures shown in Figs. 5(A) and 5(B), the reconstructive nature of the phase transition is apparent. A similar type of the reconstructive phase transition, accompanied by a drastic change of conductivity, was reported for $CsSnI_3$, in which the structure changed from a NH_4CdCl_3 type to a perovskite-type and the semiconducting conductivity increased to a metallic one at 425 K.[4]

Figure 6 shows the XRD patterns of $CH_3NH_3SnCl_3$ at selective temperatures. Although the phase transitions of $CH_3NH_3SnCl_3$ were very complicated at around 300 K, the powder pattern changed only slightly below Phase II (rhombohedral phase). The powder patterns for Phases I to IV could be analyzed by the Rietveld method. Their crystallographic parameters and experimental details are summarized in Table 1. Table 2 shows positional parameters for these phases. Although we could not decide on the space group for Phase II unequivocally from only the XRD pattern, a noncentrosymmetric space group, *R*3*m*, was adopted. This structure is consistent with ^{119}Sn NMR having a large chemical-shift anisotropy, as mentioned below. The crystal structure at Phase II is isomorphous with $CsGeBr_3$.[11] Below the rhombohedral phase, an isolated trigonal $SnCl_3^-$ anion was recognized in a distorted octahedral coordination. The dis-

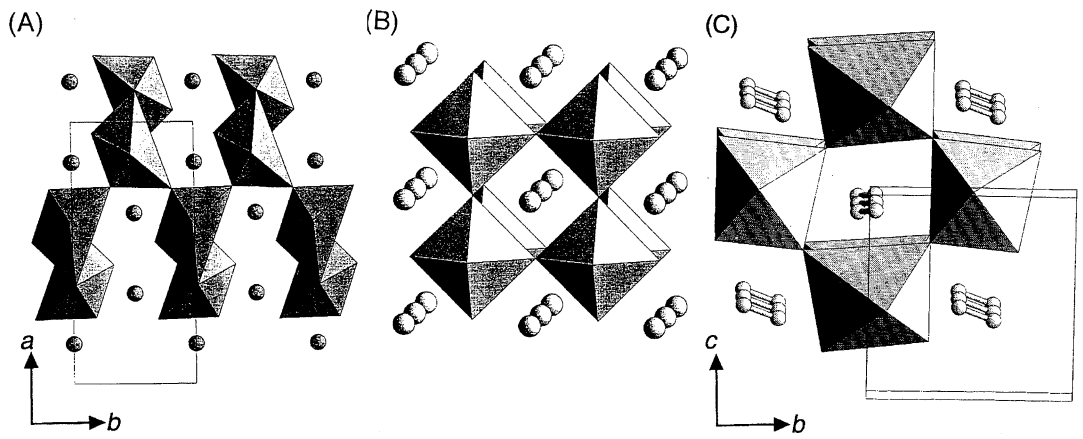

Fig. 5. Crystal structures of $CsSnCl_3$ and $CH_3NH_3SnCl_3$. (A) Phase II of $CsSnCl_3$, (B) Phase I of $CsSnCl_3$, and (C) Distorted perovskite structure of $CH_3NH_3SnCl_3$ at Phase IV.

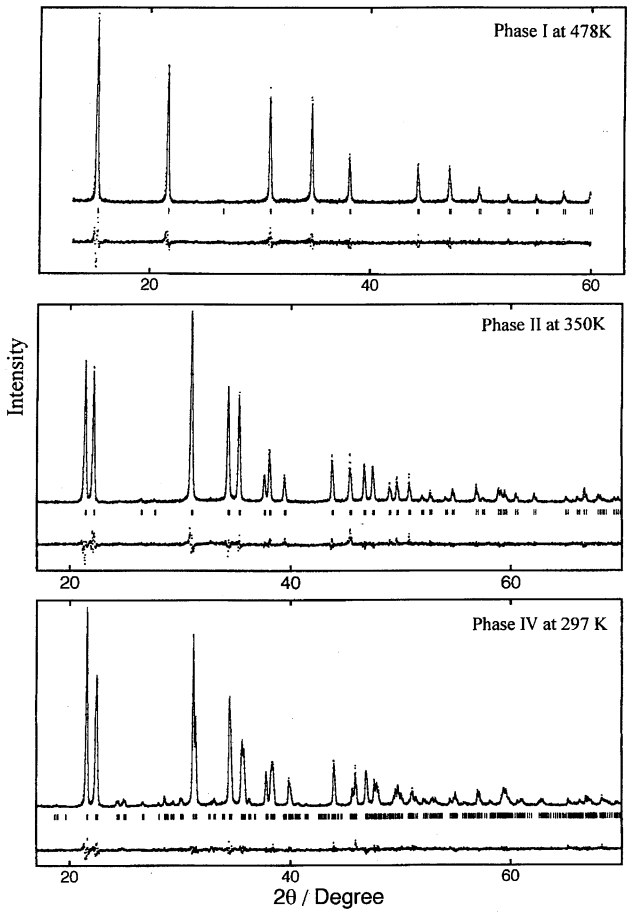

Fig. 6. Rietveld refinement plots for $CH_3NH_3SnCl_3$ at Phase I, II, and IV.

torted perovskite structure in Phase IV is shown in Fig. 4(C). In these successive phase transitions, the symmetric *trans* Cl–Sn–Cl bond in the cubic phase deforms to an asymmetric type, Cl–Sn···Cl, with decreasing temperature. This type of deformation is a common feature for trihalogenostannate(II) or trihalogenogermanate(II) salts. In the case of the $GeCl_3^-$ anion, a good correlation between Ge–Cl and Ge···Cl was found.[1] That is, a strong Ge–Cl bond leads to a weakening of the trans Ge···Cl bond, and vice versa. The semiconducting properties of these perovskite may be explained by their band structures, caused by the linear bridging bonds which form three-dimensionally throughout the crystal in the crystal lattice.

In order to examine the chloride ion diffusion in the cubic phase, we attempted a Rietveld refinement using several different models, including disordered structures. The disorder model, such as that found in $CH_3NH_3GeCl_3$, $(CH_3)_4NGeCl_3$ or $(CH_3)_4NGeBr_3$, however, could not be confirmed. Concerning the possibility of cation and/or anion diffusion we will discuss it later based on ^1H and ^{119}Sn NMR observations.

^{35}Cl NQR of $CsSnCl_3$. Three ^{35}Cl NQR signals could be detected in Phase II of $CsSnCl_3$. Since only a broad spin-echo signal centered at 10.40 MHz (FWHM=300 kHz) could be detected for Phase I*, no further NQR experiment could be performed. Figure 7 shows the temperature dependence of the NQR frequency and its spin-lattice relaxation time for Phase II of Cs salt. Three ^{35}Cl NQR frequencies agreed well with those reported by Scaife et al.[12] Just below the phase transition at 379 K, the relaxation rate ($1/T_1$) increased exponentially with the temperature. The temperature dependence of the relaxation rate assigned to the ν_2 line could be satisfactorily reproduced using

$$1/(T_1/\mathrm{s}) = 5.75\cdot10^{-5}\cdot T^{2.02} + 1.32\cdot10^{12}\cdot\exp(-62.8\ \mathrm{kJ\,mol^{-1}}/RT). \quad (1)$$

The first term represents a Raman process, and is almost proportional to T^2, as expected from the mechanism.[14] The second term represents a contribution from a reorientation of the group containing probe nucleus. The activation energy, 62.8 kJ mol^{-1}, was assigned to the reorientation of $SnCl_3^-$ anions around its pseudo C_3 axis, because an isolated anion was recognized in Phase II. The reorientation of the $SnCl_3^-$ anion should be the largest driving force for the transition to the cubic phase. Unfortunately, no NQR signal was observed for $CH_3NH_3SnCl_3$.

Dynamic Structure of $CH_3NH_3SnCl_3$ Studied by ^1H, ^2H, and ^{119}Sn NMR Spectroscopy. In order to obtained the dynamical information about $CH_3NH_3SnCl_3$, broadline ^1H, ^2H, and ^{119}Sn NMR spectroscopies were employed. Figure 8 shows the temperature dependencies of the spin-lattice relaxation times of ^2H NMR for $CH_3N^2H_3SnCl_3$ together with their spectra at selective temperatures. Since the quadrupole splitting of ^2H for a rigid N^2H_3 group was reported to be ca. 120 kHz, the observed splitting of 41 kHz with a negligible asymmetry parameter at 77 K suggested a reorientation of the N^2H_3 group about the C–N bond. When the temperature increased, the quadrupole splitting gradually decreased, and became almost zero above the phase transition to the rhombohedral phase. An overall reorientation of the cation is existed in this phase. A residual splitting of about 3 kHz may be due to the fact that the reorientation is not perfectly isotropic in the rhombohedral lattice. From these findings, the phase transition at 331 K can be considered to have an orientational order–disorder character of the cation. On the other hand, the BPP formula of the spin-lattice relaxation times for $I>1/2$ nucleus is

$$1/T_1 = \frac{3(2I+3)}{40I^2(2I-1)}\left(1+\eta^2/3\right)\left(e^2Qq/h\right)^2\left[\tau_c/\left(1+\omega^2\tau_c^2\right)\right], \quad (2)$$

where ω is the Lormor frequency, I the spin quantum number, τ_c the correlation time of the motion, e^2Qq/h the quadrupole coupling constant being modulated with time constant τ_c and η the asymmetry parameter of the quadrupole interaction. Since the observed T_1 increased with temperature, a fast-motion limit, $\omega\tau_c \ll 1$, can be applied to Eq. 2, reducing it to

$$1/T_1 = (3/40)\left(1+\eta^2/3\right)\left(e^2Qq/h\right)^2\tau_c. \quad (3)$$

Assuming an Arrhenius equation for τ_c, the activation energy for the reorientation was determined to be 2.2 and 17.7 kJ mol^{-1} below and above 331 K, respectively. These activation energies correspond to the uniaxial reorientation

Table 1. Crystallographic Data and Experimental Details for the Rietveld Refinements of $CsSnCl_3$ (Phase I) and $CH_3NH_3SnCl_3$ (Phase I—IV)

Compound	$CsSnCl_3$	$CH_3NH_3SnCl_3$			
Phase	I	I	II	III	IV
Temperature/K	413	478	350	318	297
Space group	$Pm\bar{3}m$ (No.221)	$Pm\bar{3}m$ (No.221)	$R3m$ (No.160)	Pc (No.7)	$P1$ (No.1)
Crystal system	Cubic	Cubic	Rhombohedral	Monoclinic	Triclinic
Lattice parameters	$a=5.604(1)$ Å	$a=5.760(1)$ Å	$a=5.734(1)$ Å $\alpha=91.90(1)°$	$a=5.718(1)$ Å $b=8.236(1)$ Å $c=7.938(1)$ Å $\beta=93.03(1)°$	$a=5.726$ Å $b=8.227$ Å $c=7.910$ Å $\alpha=90.40°$ $\beta=93.08°$ $\gamma=90.15°$
Z	1	1	1	2	2
Calcd density/g cm^{-3}	3.38	2.23	2.27	2.29	2.30
Number of parameters	20	20	23	40	64
2θ for refinement	10°— 60°	10°— 60°	17°— 80°	17°— 80°	17°— 80°
R_p[a)]	0.085	0.148	0.097	0.091	0.072
R_{wp}[b)]	0.111	0.203	0.128	0.119	0.098
R_e[c)]	0.103	0.119	0.134	0.134	0.111
R_F[d)]	0.040	0.037	0.040	0.036	0.026
DS, RS, SS[e)]	0.5°, 0.15 mm, 0.5°	0.5°, 0.15 mm, 0.5°	1.0°, 0.3 mm, 1.0°	1.0°, 0.3 mm, 1.0°	1.0°, 0.3 mm, 1.0°

a) $R_p=\sum|y_i(\mathrm{obs})-y_i(\mathrm{cal})|/\sum y_i(\mathrm{obs})$, where $y_i(\mathrm{obs})$ and $y_i(\mathrm{cal})$ are the observed and calculated intensities at ith steps.
b) $R_{wp}=(\sum w_i(y_i(\mathrm{obs})-y_i(\mathrm{cal}))^2/\sum w_i(y_i(\mathrm{obs}))^2)^{1/2}$, where $w_i=1/y_i(\mathrm{obs})$. c) $R_F=\sum|(I_K(\mathrm{obs}))^{1/2}-(I_K(\mathrm{cal}))^{1/2}|/\sum(I_K(\mathrm{obs}))^{1/2}$, I_K is the intensity assigned to the Kth Bragg reflection. d) R_e (expected R factor) $=((N-P)/\sum w_i y_i(\mathrm{obs}))^{1/2}$, where N and P are numbers of data and parameters, respectively. e) Divergence slit, receiving slit and scatter slit.

Table 2. Positional Parameters for $CH_3NH_3SnCl_3$ at Phase I, II, III, and IV

Phase	Atom	Site symmetry[b)]	x	y	z	B_{iso}/Å^2
	CH_3NH_3[a)]	$m\bar{3}m$	0.0	0.0	0.0	34(11)
Phase I	Sn	$m\bar{3}m$	0.5	0.5	0.5	4(1)
(478 K)	Cl	4/*mmm*	0.0	0.5	0.5	13(4)
	CH_3NH_3	3*m*	0.008(15)	$=x$	$=x$	45.3(11)
Phase II	Sn	3*m*	0.500	0.500	0.500	3.1(1)
(350 K)	Cl	*m*	−0.009(16)	0.479(5)	$=y$	14.3(3)
	C or N(1)	1	0.245(8)	0.299(7)	0.469(5)	17.8(13)
	C or N(2)	1	0.001(7)	0.242(9)	0.490(14)	17.8
Phase III	Sn	1	0.500	0.2515(6)	0.000	3.0(1)
(318 K)	Cl(1)	1	0.426(6)	−0.024(3)	0.272(4)	9.8(5)
	Cl(2)	1	0.506(5)	0.485(5)	0.300(3)	9.8
	Cl(3)	1	0.050(1)	0.294(4)	−0.001(5)	9.8
	C or N(1)	1	0.825(11)	0.023(8)	0.031(7)	14.2(10)
	C or N(2)	1	1.061(11)	−0.058(8)	0.048(7)	14.2
	C or N(3)	1	−0.029(11)	0.582(8)	0.571(8)	14.2
	C or N(4)	1	−0.116(14)	0.420(9)	0.505(8)	14.2
Phase IV	Sn(1)	1	0.500	0.500	0.000	2.9(2)
(297 K)	Sn(2)	1	0.487(2)	−0.001(1)	0.507(1)	2.8(2)
	Cl(1)	1	0.522(4)	0.282(3)	0.215(3)	3.1(8)
	Cl(2)	1	−0.076(4)	0.083(3)	0.529(3)	2.5(6)
	Cl(3)	1	−0.055(4)	0.479(3)	−0.060(4)	3.3(8)
	Cl(4)	1	0.564(7)	0.694(3)	0.259(4)	8.1(9)
	Cl(5)	1	0.493(5)	0.284(4)	0.698(4)	5.3(9)
	Cl(6)	1	0.583(4)	0.789(3)	0.758(3)	3.8(8)

a) Isoelectronic dummy atom K^+ was used for the refinement due to the isotropic reorientation. b) Wyckoff nation.

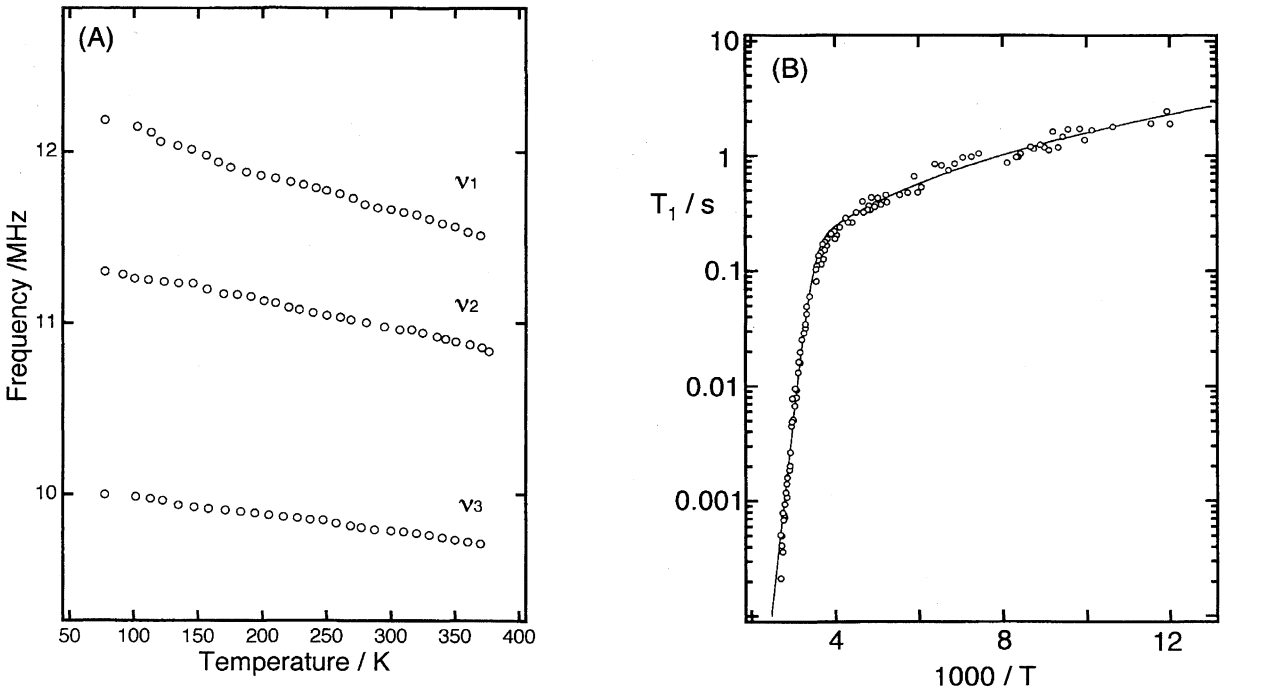

Fig. 7. Temperature dependence of (A) ^{35}Cl NQR frequencies and (B) spin-lattice relaxation times for $CsSnCl_3$.

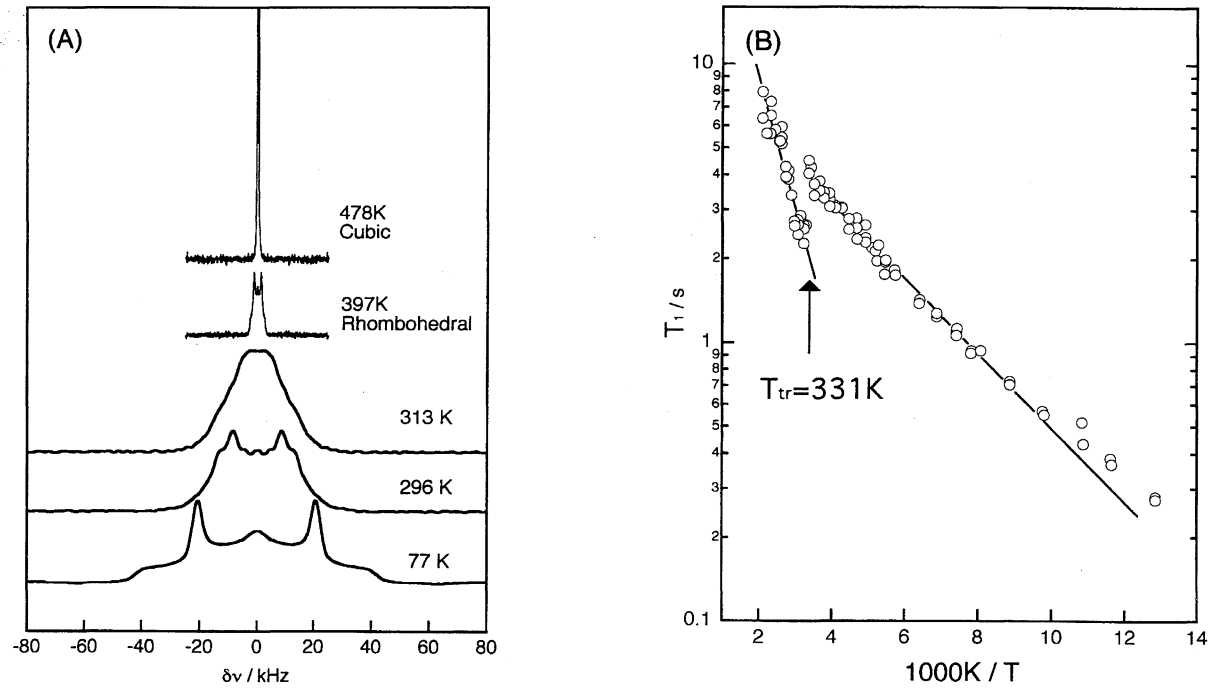

Fig. 8. Temperature dependence of (A) ^{2}H NMR spectra and (B) spin-lattice relaxation times for $CH_3N^2H_3SnCl_3$.

of the $CH_3NH_3^+$ around the C_3 axis and the isotropic overall reorientation of the cation. Quite similar T_1 behaviors were observed for $CH_3NH_3PbX_3$, in which the motions of the monomethylammonium ions in the perovskite lattices were studied by ^{1}H NMR in detail.[14]

^{1}H NMR is more straightforward than ^{2}N NMR to detect the translational diffusion of the cation, because the linewidth due to dipole–dipole interactions in ^{1}H NMR reduces considerably at the beginning of the diffusion. In the temperature range between 300 and 400 K, the linewidth (peak-to-peak linewidth of the derivative of the absorption curve) was 1.8 Gauss and almost constant. The corresponding second moment was calculated to be 0.5 Gauss^2, suggesting an isotropic reorientation of the cation with a time scale $>10^4$ Hz. Above 450 K, which is just below the phase transition to the cubic phase, a small fraction of a sharp component appeared on the absorption line. This finding suggested that a part of the cations probably began to diffuse due to a point defect

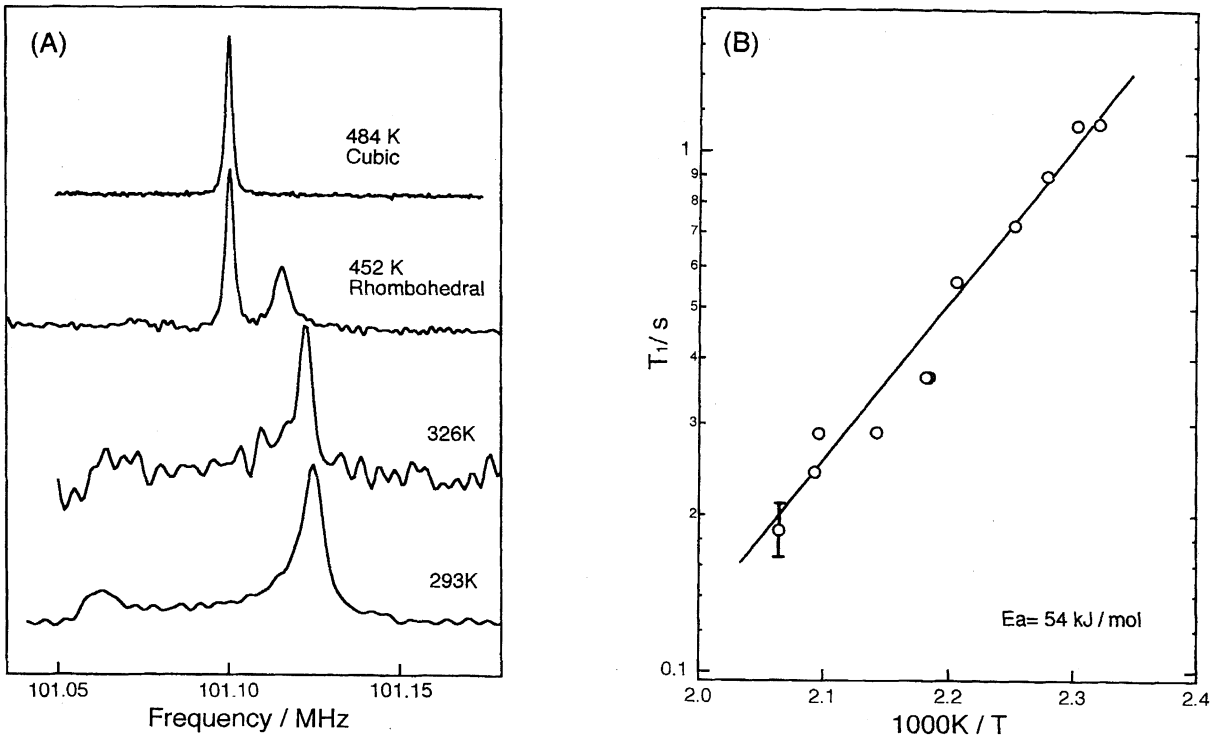

Fig. 9. Temperature dependence of (A) ^{119}Sn NMR spectra and (B) spin-lattice relaxation times for $CH_3NH_3SnCl_3$.

created thermally.

The possibility of ionic conductivity due to chloride ions was investigated by means of ^{119}Sn NMR experiments. Figure 9(A) shows the ^{119}Sn spectra for $CH_3NH_3SnCl_3$ at the selective temperatures. Figure 9(B) shows the temperature dependence of their spin-lattice relaxation times above the rhombohedral phase. In the case of $CsSnCl_3$, the powder pattern having an axial chemical-shift tensor changed to a sharp singlet at T_{tr}, as expected from the cubic structure. The chemical-shift anisotropy was determined to be 860 ppm for an isolated $SnCl_3^-$ anion in $CsSnCl_3$ at 298 K. On the other hand, the anisotropy for $CH_3NH_3SnCl_3$ was determined to be 631 ppm, which was 73% of that of $CsSnCl_3$. Since the chemical-shift anisotropy is a measure of the isolation of the pyramidal $SnCl_3^-$ anion, the interanionic interactions in CH_3NH_3 salt are stronger than those in Cs salt. With increasing temperature, a sharp component appeared having no chemical-shift anisotropy, even in the rhombohedral phase, similar to the ^{1}H NMR spectrum. This partial averaging effect of the chemical shift may suggest the onset of chloride-ion diffusion using a point defect which was generated thermally. In order to estimate the activation energy for the diffusion, the spin-lattice relaxation times of ^{119}Sn NMR were measured above 431 K, while monitoring the sharp component at the center. Since the time-dependent chemical-shift interaction affects the relaxation of the Zeeman energy, the form of the T_1 is expressed as[15]

$$1/T_1 = (2/15)\,\gamma^2 B_0^2 \delta^2 \left[\tau_c / \left(1+\omega^2\tau_c^2\right)\right]. \quad (4)$$

In this equation γ is a gyromagnetic ratio, B_0 the magnetic field and δ the chemical-shift anisotropy, $\delta = \sigma_{33} - \sigma_{iso}$. Since there is no discontinuity in the T_1 vs. $1/T$ plot, we assumed that the same mechanism governed the relaxation rate above 421 K. Assuming an Arrhenius equation for τ_c and a slow-motion limit ($\omega\tau_c \gg 1$), the activation energy for the diffusion of chloride ions was determined to be 54 kJ mol^{-1}. This activation energy is about 2-times larger than that of cubic $CH_3NH_3GeCl_3$ in which chloride-ion diffusion takes place between the disordered sites. Furthermore, the estimated ionic conductivity from the NMR parameters due to the anion and/or cation diffusion was lower by several orders than the observed one. This is consistent with a polarization measurement which suggests a semiconducting property of $CH_3NH_3SnCl_3$.

This work was supported by a Grant-in-Aid for Scientific Research on Priority Areas of "Solid State Ionics", No. 09215226 and by a Grant-in-Aid for Scientific Research No. 09640690 from the Ministry of Education, Science, Sports and Culture.

References

1) K. Yamada, K. Isobe, T. Okuda, and Y. Furukawa, *Z. Naturforsch., A*, **49a**, 258 (1994).

2) K. Yamada, K. Isobe, E. Tsuyama, T. Okuda, and Y. Furukawa, *Solid State Ionics*, **79**, 152 (1995).

3) K. Yamada, T. Matsui, T. Tsuritani, T. Okuda, and S. Ichiba, *Z. Naturforsch., A*, **45a**, 307 (1990).

4) K. Yamada, S. Funabiki, H. Horimoto, T. Matsui, T. Okuda, and S. Ichiba, *Chem. Lett.*, **1991**, 801.

5) K. Yamada, H. Kawaguchi, T. Matsui, T. Okuda, and S.

Ichiba, *Bull. Chem. Soc. Jpn.*, **63**, 2521 (1990).

6) T. Okuda, S. Goto, T. Takahashi, H. Terao, and K. Yamada, *Z. Naturforsch.*, *A*, **51a**, 686 (1996).

7) F. Izumi, in "The Rietveld Method," ed by R. A. Young, Oxford University Press, Oxford (1993), p. 236.

8) K. Yamada, S. Nose, T. Umehara, T. Okuda, and S. Ichiba, *Bull. Chem. Soc. Jpn.*, **61**, 4265 (1988).

9) F. R. Poulson and S. E. Rasmussen, *Acta Chem. Scand.*, **24**, 150 (1970).

10) S. Sharma, N. Weiden, and A. Weiss, *Z. Naturforsch.*, *A*, **46a**, 329 (1991).

11) G. Thiele, H. W. Rotter, and K. D. Schmidt, *Z. Anorg. Allg. Chem.*, **559**, 7 (1988).

12) D. E. Scaife, P. W. Weller, and W. G. Fisher, *J. Solid State Chem.*, **9**, 308 (1974).

13) H. Chihara and N. Nakamura, "Advances in Nuclear Quadrupole Resonance," ed by J. A. S. Smith, Heyden & Son, Ltd., London (1980), Vol. 4, p. 1.

14) Q. Xu, T. Eguchi, H. Nakayama, and N. Nakamura, *Z. Naturforsch.*, *A*, **46a**, 240 (1991).

15) B. C. Cerstein and C. R. Dybowski, "Transient Techniques in NMR of Solids," Academic Press, Inc., New York (1985), p. 132.